Demonstration of meta-signal positioning using LAMBDA ambiguity fixing method within a bit-true simulation

Muhammad S. Hameed, *Universität der Bundeswehr München*
Thomas Woerz, *Airbus Defence and Space GmbH*
Thomas Pany, *Universität der Bundeswehr München*
Jan Wendel, *Airbus Defence and Space GmbH*
Matteo Paonni, *European Commission, Joint Research Centre, Ispra*
Tommaso Senni, *Technical Advisor for the European Commission*

BIOGRAPHY

Muhammad S. Hameed received a bachelor in Electrical Engineering in 2016 from the National University of Sciences and Technology (NUST), Pakistan and a master in Earth Oriented Space Science and Technology (ESPACE) in 2020 from the Technical University of Munich (TUM), Germany. He has been working as a research associate at the Institute of Space Technology and Space Applications of the Universität der Bundeswehr München. His current research interests include GNSS receiver technology, signal generation and signal tracking performance analysis.

Thomas Woerz received a Diploma degree in 1988 from the Technical University of Stuttgart and a Doctoral degree in 1995 from the Technical University of Munich, respectively. From 1988 to 1998 he was a member of the research staff at the German Aerospace Center. He co-founded AUDENS ACT Consulting GmbH in 1998. He is currently working as Senior GNSS Signal Engineer at Airbus Defence and Space GmbH in Ottobrunn, Germany.

Thomas Pany is with the Universität der Bundeswehr München at the faculty of aerospace engineering and leads the navigation group within Institute of Space Technology and Space Applications (ISTA). He is working with GNSS since 1997 and with software radio technology since 2002. He has around 200 publications including one book and five patents.

Jan Wendel received the Dipl.-Ing. and Dr.-Ing. degrees in Electrical Engineering from the University of Karlsruhe, Germany, in 1998 and 2003, respectively. From 2003 until 2006 he was an assistant professor at the University of Karlsruhe, where he was private lecturer until 2018. In 2006, Jan Wendel joined MBDA in Munich, Germany, working on the development of navigation algorithms for various applications. In 2009, he joined Airbus Defence and Space in Munich, where he is involved in various activities related to satellite navigation including acquisition and tracking algorithms, interference detection and characterisation, integrity algorithms, and PRS receiver development.

Matteo Paonni is a team leader within the Directorate for Space, Security and Migration at Joint Research Centre of the European Commission in Ispra, Italy. Under his position Matteo provides technical and policy support on the EU Satellite Navigation Programmes to DG DEFIS and the EU Agency for the Space Programme (EUSPA). Matteo's main focus is on GNSS signal design and optimization, GNSS compatibility and GNSS signal processing. From 2007 to 2013 he was a research associate at the Institute of Space Technology and Space Applications at the University of the Federal Armed Forces in Munich.

Tommaso Senni earned his B.Sc. degree in electronic engineering from Perugia University and his M.Sc. degree in telecommunication engineering from Universita degli Studi di Roma. Currently, he is the EGNSS signal advisor at the European Commission DG GROW, where he works on the definition of Galileo first generation and second generation services. He is a system engineer specializing in satellite navigation systems with experience in GNSS systems, GNSS applications, and signal processing. He has been a SIS engineer at the ESA/ESTEC and a system engineer at IFEN GmbH and Space Engineering, S.p.a.

ABSTRACT

The prospect of tracking two signals on different carrier frequencies as one wideband signal is often referred to as meta-signal tracking. The general interest in meta-signals is derived from the fact that the correlation function of such a signal consists of a narrower main peak than the correlation functions of its constituent signals which implies that with an adapted signal tracking architecture, such as the Double Estimator, the meta-signal can be tracked with small tracking jitter and better multipath rejection performance ultimately producing position solutions with improved accuracy. To validate and demonstrate this, as part

of FUNTIMES2 Horizon 2020 (H2020) RD Framework project, a complete GNSS processing chain is employed which consists of a fully realistic bit-true GNSS signal generation done at the IF sample level, GNSS SDR processing and positioning using an engine that implements an adapted LAMBDA ambiguity fixing method. The signal generation is done using PIPE simulation tool chain from Airbus Defence and Space GmbH with an assumed signal structure. The LAMBDA-method is adapted to resolve sub-carrier ambiguities by implementing a Kalman filter which uses code and sub-carrier pseudorange measurements which are obtained from a PIPE-generated RINEX observation file and are used to update the filter state-vector at each epoch. The filter produces a float solution, which is passed onto a dedicated LAMBDA ambiguity resolution block to produce a fixed solution, which is then conditionally used to update the estimated receiver position with accuracy up to the cm level.

I. INTRODUCTION TO META-SIGNAL TRACKING

Meta-signal tracking corresponds to the prospect of tracking two signals that are transmitted on different carrier frequencies as one wide-band signal [1] [2]. This can be done by adopting a tracking architecture that, besides tracking the code and carrier phase, keeps a track on the frequency offset between the two signals. This can be realized either by using a modified Double-estimator tracking architecture which uses a dedicated frequency offset tracking loop or by coupling two conventional receiver channels in a master-slave configuration so that the slave channel shares the same carrier NCO as the master channel.

The correlation function of a meta-signal highly resembles the correlation function of a high-order BOC signal in the sense that the main correlation peak is very narrow and that there exists several other narrow side-peaks as stable tracking points. Hence, a given meta-signal can be approximated as a high-order BOC signal which invokes interest in optimal high-order BOC tracking schemes, some of which are briefly discussed, in the following sub-section.

1. High-order BOC tracking

In tracking of GNSS signals a phase lock loop (PLL) is used for carrier tracking and a delay lock loop (DLL) is used for code tracking. The PLL performs a carrier wipe-off, so that the signal after multiplication with the carrier replica generated by the carrier numerically controlled oscillator (NCO) only consists of the modulated PRN code chips. The modulation function for the PRN code chips can be a rectangular function in the case of BPSK or a sinusoisal sub-carrier in the case of BOC. For BPSK modulation, the auto-correlation function (ACF) is triangular having only one stable tracking point, hence, making it sufficient to use a three correlator (Early-Prompt-Late) DLL in which the Prompt correlator is aligned to the stable tracking point by advancing/delaying all the correlators based on the output of a DLL discriminator function.

a). Bump Jump

For BOC modulation [3], besides the tracking point on the main peak, the ACF consists of several other stable tracking points due to the presence of side-peaks. This firstly invokes to choose the early-late spacing appropriately so that only the main peak is covered by the primary three correlators. Secondly, to avoid false lock onto any of the side-peaks, a Bump Jump scheme can be implemented which employs two additional correlators: the Very Early (VE) and Very Late (VL) correlators [4]. A false lock is said to be occurring if there exists a significant difference between the VE and VL correlator values over a given time duration. For low-order BOC signals, the amplitude difference between consecutive side-peaks is high enough for the Bump Jump algorithm to correctly recognise false locks. However, in the case of high-order BOC signals, the amplitudes of consecutive side-peaks only slightly differ. Hence, the Bump Jump algorithm does not recognize false locks for high order BOC signals [5], with the same success rate, as for low-order BOC signals.

b). Double Estimator

In a Double Estimator tracking structure, besides the conventional PLL and DLL, a Sub-carrier Lock Loop is implemented [6]. The SLL uses a sub-carrier replica for correlation after the PRN code is wiped-off by the DLL. Using SLL code phase, the sub-carrier pseudoranges are obtained which are very precise but ambiguous i.e the tracking jitter in the SLL output is very small but the tracked sub-carrier position within a given PRN code sequence is not known. If the DLL measurement noise is within a half sub-carrier wavelength, then the code pseudorange measurements can directly be used to resolve sub-carrier ambiguities, however, in the case of realistic channel conditions this, the code observations are additionally corrupted by multipath and other parasitic effects. Hence, in the absence of ambiguity fixing filter, the Double Estimator scheme alone is ineffective especially when there is high code noise for e.g in urban canyon environments.

2. Sub-carrier ambiguity resolution in position domain

By employing a Double-Estimator like tracking structure for meta-signal, sub-carrier observations can be obtained at the SLL output. The presence of ambiguity in sub-carrier observations is analogues to the presence of ambiguity in carrier-phase observations. However, since the sub-carrier wavelength of a meta-signal is in the order of 10 to 15 m [7], which is much larger than the carrier wavelength which is in the order of 20 cm, it is possible to resolve sub-carrier ambiguities by conditioning

sub-carrier observations on filtered code observations without having the need of a reference station. This can be realized by using a combined code and sub-carrier observation model within a filter set-up. Hence, with meta-signal positioning, position solutions which are accurate up to the cm level, can potentially be obtained by using a single receiver provided that the satellite orbits, clocks and atmospheric delays are modelled at the same precision. Overall, the target market of this technology covers the GNSS receivers used in commercial low-cost hand-held devices such as smart phones that occupy 90 percent of the market share for GNSS receivers costing less than 5 € and is expected to increase with almost 1.8 billion Smartphones by 2029 [8].

II. META-SIGNAL POSITIONING ENGINE

Within the meta-signal positioning engine, illustrated in Fig. 1, a closed-loop Kalman filter is implemented, in which at each epoch code and sub-carrier pseudorange measurements, obtained from a RINEX [9] observation file, are used to update the filter state-vector. The filter state-vector produces a float solution, which is then passed onto a dedicated LAMBDA ambiguity resolution block as input. This block performs sub-carrier ambiguity resolution to produce a fixed solution, which is conditionally used to update the estimated receiver position.

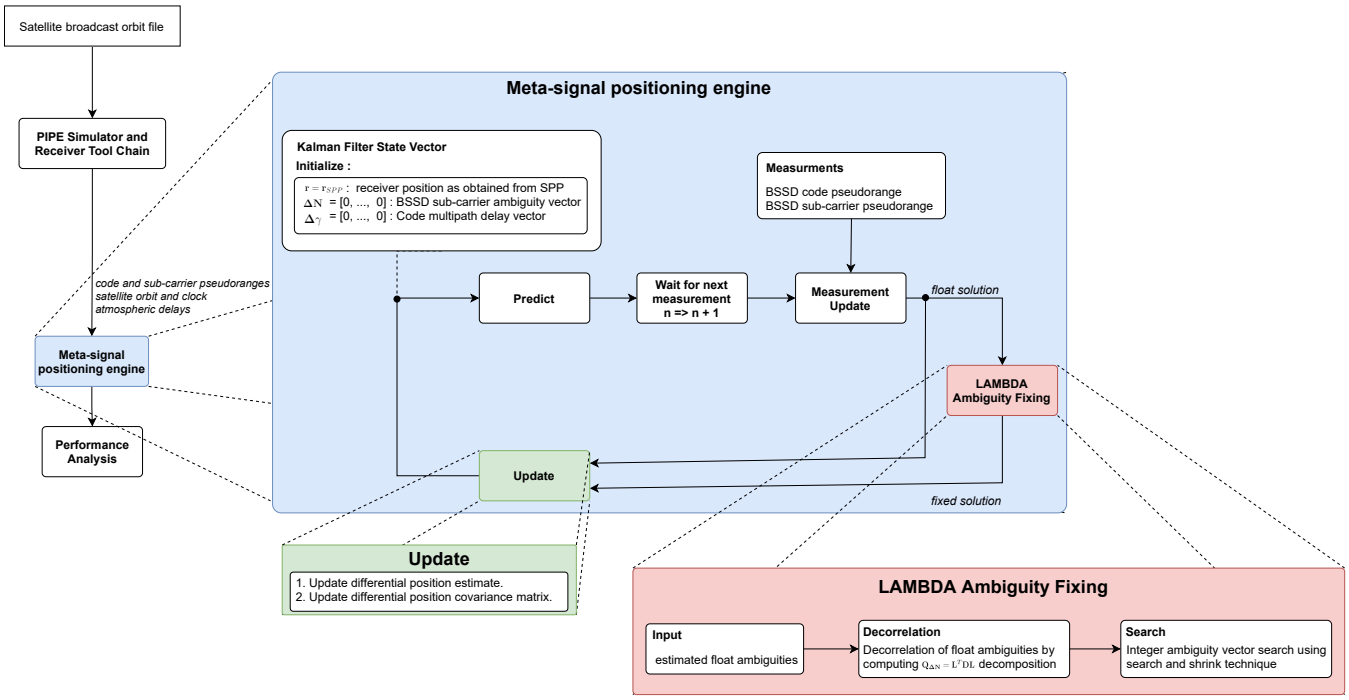

Figure 1: Meta-signal positioning engine block diagram

1. Observation model

We consider a single frequency system with K valid satellites visible to the receiver in the observation window. Also, this is a single receiver scenario where the absolute receiver position is estimated. For this system, the code and sub-carrier observation models given in Eqn. 1 and 2 are considered.

$$\widetilde{\rho}^k = \left|\left|\vec{\mathbf{r}^k} - \vec{\mathbf{r}}\right|\right| + c\left(\delta\tau - (\delta\tau^k + \delta\tau^k_{rel})\right) + T^k + I^k + \gamma^k + \nu^k_\rho \tag{1}$$

$$\widetilde{\phi}^k = \left|\left|\vec{\mathbf{r}^k} - \vec{\mathbf{r}}\right|\right| + c\left(\delta\tau - (\delta\tau^k + \delta\tau^k_{rel})\right) + N^k\lambda + T^k + I^k + \nu^k_\phi \tag{2}$$

where $\vec{\mathbf{r}^k}$ is the satellite position, $\vec{\mathbf{r}}$ is the receiver position, c is the speed of light, $\delta\tau$ is the receiver clock offset, $\delta\tau^k$ is the satellite clock offset, $\delta\tau^k_{rel}$ is the satellite clock relativity term and T^k and I^k are tropospheric and ionospheric delays in meters, respectively. γ^k is the code multipath delay. ν^k_ρ and ν^k_ϕ represent the code and sub-carrier noise, respectively. The sub-carrier pseudorange is ambiguous by $N^k\lambda$ meters where N^k is the integer ambiguity to be resolved and λ is the sub-carrier wavelength.

Considering the troposphere and ionospheric delays to be known as a prior with sufficient precision through atmospheric models, the corrected code and sub-carrier observations are expressed as in Eqn. 3 and 4 where ρ^k and ϕ^k are the modeled code and sub-carrier pseudoranges respectively. In order to eliminate the receiver clock offset, Between-Satellite-Single-Difference (BSSD) is taken with respect to a reference satellite. The satellite having the highest elevation angle is considered as the reference satellite, and therefore, the index 0 is assigned to it. The BSSD observation is formulated as in Eqn. 5 and 6 for code and sub-carrier respectively.

$$\widetilde{\rho}^k - \rho^k = -\left(\vec{\mathbf{e}^k}\right)^{\mathbf{T}} \vec{\mathbf{r}} + c\delta\tau \; + \gamma^k + \; \nu_\rho^k \tag{3}$$

$$\widetilde{\phi}^k - \phi^k = -\left(\vec{\mathbf{e}^k}\right)^{\mathbf{T}} \vec{\mathbf{r}} + c\delta\tau \; + \; N^k\lambda + \nu_\phi^k \tag{4}$$

$$\bar{\rho^k} = (\widetilde{\rho}^k - \rho^k) - (\widetilde{\rho}^0 - \rho^0) = -\left(\left(\vec{\mathbf{e}^k}\right)^T + \left(\vec{\mathbf{e}^0}\right)^T\right)\vec{\mathbf{r}} + \Delta\gamma^k + \nu_\rho^k - \nu_\rho^0 \tag{5}$$

$$\bar{\phi^k} = \left(\widetilde{\phi}^k - \phi^k\right) - \left(\widetilde{\phi}^0 - \phi^0\right) = -\left(\left(\vec{\mathbf{e}^k}\right)^T + \left(\vec{\mathbf{e}^0}\right)^T\right)\vec{\mathbf{r}} + \Delta N^k\lambda + \nu_\phi^k - \nu_\phi^0 \tag{6}$$

The combined BSSD code and sub-carrier observation model, as expressed in Eqn. 7, is used as the system model within the Kalman filter. In this combined observation model $\mathbf{y}$ is the BSSD measurement vector, $\mathbf{H}$ is the geometry matrix, $\mathbf{A}_\lambda$ is the state-coefficient matrix for the BSSD sub-carrier ambiguity vector $\mathbf{\Delta N}$, $\mathbf{A}_\gamma$ is the state-coefficient matrix for the BSSD code multipath vector $\mathbf{\Delta}\gamma$.

$$\mathbf{y} = \mathbf{H}\vec{\mathbf{r}} + \mathbf{A}\begin{pmatrix}\mathbf{\Delta N}\\ \mathbf{\Delta}\gamma\end{pmatrix} + \epsilon_{\mathbf{y}} \tag{7}$$

$$\mathbf{y} = \begin{pmatrix}\bar{\rho^1}\\ .\\ .\\ \bar{\rho^k}\\ \bar{\phi^1}\\ .\\ .\\ \bar{\phi^k}\end{pmatrix} \tag{8}$$

$$\mathbf{\Delta N} = \begin{pmatrix}\Delta N^1\\ .\\ .\\ \Delta N^{K-1}\end{pmatrix} \tag{9}$$

$$\mathbf{\Delta}\gamma = \begin{pmatrix}\Delta\gamma^1\\ .\\ .\\ \Delta\gamma^{K-1}\end{pmatrix} \tag{10}$$

$$\mathbf{H} = \begin{pmatrix} -\left(\left(\vec{\mathbf{e}^1}\right)^T + \left(\vec{\mathbf{e}^0}\right)^T\right)\\ .\\ .\\ -\left(\left(\vec{\mathbf{e}^{K-1}}\right)^T + \left(\vec{\mathbf{e}^0}\right)^T\right)\\ -\left(\left(\vec{\mathbf{e}^1}\right)^T + \left(\vec{\mathbf{e}^0}\right)^T\right)\\ .\\ .\\ -\left(\left(\vec{\mathbf{e}^{K-1}}\right)^T + \left(\vec{\mathbf{e}^0}\right)^T\right)\end{pmatrix} \tag{11}$$

$$\mathbf{A}_\lambda = \begin{pmatrix}\mathbf{0}_{(K-1)(K-1)}\\ \lambda\mathbf{I}_{(K-1)(K-1)}\end{pmatrix} \tag{12}$$

$$\mathbf{A}_\gamma = \begin{pmatrix}\mathbf{I}_{(K-1)(K-1)}\\ \mathbf{0}_{(K-1)(K-1)}\end{pmatrix} \tag{13}$$

$$\mathbf{A} = (\mathbf{A}_\lambda, \mathbf{A}_\gamma) \tag{14}$$

$$\mathbf{F} = (\mathbf{H}, \mathbf{A}) \tag{15}$$

2. Kalman filter

For positioning, a Kalman filter is used to estimate the differential offsets to absolute receiver position, the BSSD ambiguities and BSSD code multipath in each epoch. The filter state-vector $\mathbf{x}$ is given in Eqn. 16 where $\delta x, \delta y$ and δz are the position offset states, $\delta\Delta N^k$ and $\delta\Delta\gamma^k$ are the BSSD sub-carrier ambiguity and code multipath offset state respectively for satellite k.

In each epoch and for every satellite, after obtaining the raw code and sub-carrier pseudoranges, the corrected pseudorange observations are formed by compensating for satellite clock offset and the known atmospheric delays. Thus this simulation refers to a (future) scenario where highly accurate ionospheric models are available in real-time. They may stem from a regional or global precise point positioning (PPP) service.

After applying these compensations, the corrected code pseudorange contains the geometry term, receiver clock offset, code multipath delay and code measurement noise. The corrected sub-carrier pseudorange contains the geometry term, receiver clock offset, an integer-wavelength ambiguity, and the sub-carrier measurement noise. To eliminate the receiver clock offset, BSSD observations are computed by considering a reference satellite. These BSSD observations formulate the the Kalman filter measurement vector $\mathbf{y}$.

$$\mathbf{x} = \begin{pmatrix} \delta x \\ \delta y \\ \delta z \\ \delta\Delta N^1 \\ . \\ . \\ \delta\Delta N^{K-1} \\ \delta\Delta\gamma^1 \\ . \\ . \\ \delta\Delta\gamma^{K-1} \end{pmatrix} \tag{16}$$

The geometry matrix $\mathbf{H}$ and the state-coeffecient matrix $\mathbf{A}$ are used to form the filter system matrix $\mathbf{F}$. The filter transition matrix $\mathbf{B}$ is a $(K-1)$ by $(K-1)$ identity matrix. The filter state covariance matrix $\mathbf{P}$ is initialized with the position state variances $\sigma^2_{dx}, \sigma^2_{dy}$ and σ^2_{dz}, the sub-carrier ambiguity state variances $\sigma^2_{N^1}, \ldots, \sigma^2_{N^{K-1}}$ and the code multipath state variances $\sigma^2_{\gamma^1}, ..., \sigma^2_{\gamma^{K-1}}$. The filter process noise matrix $\mathbf{Q}$ is initialized with the position process noise Φ_r, the sub-carrier ambiguity process noise $\Phi_{\Delta N}$ and the code multipath process noise Φ_γ. The filter measurement noise matrix $\mathbf{R}$ is initialized with code noise variance σ^2_ρ and sub-carrier noise variance σ^2_ϕ respectively.

In each epoch of the Kalman filter a time-update step propagates the state-covariance $\mathbf{P}$, as estimated from the previous time step, to the current time step with the addition of filter process noise $\mathbf{Q}$. A measurement update step computes the filter residual $\mathbf{z}$ by using the current measurement. The residual is scaled by the filter gain $\mathbf{K}$ to eventually update the state vector $\mathbf{x}$. The state-vector, at the end of each measurement update step, contains the differential estimates for the state-variables. Using these state estimates, the float solution for estimated receiver position $\vec{\mathbf{r}}$, the BSSD sub-carrier ambiguities $\mathbf{\Delta N}$ and the BSSD code multipath delay $\mathbf{\Delta}\gamma$ is obtained.

$$\mathbf{Q} = \begin{pmatrix} \Phi_r & & & & & & & & \\ & \Phi_r & & & & & & & \\ & & \Phi_r & & & \mathbf{0} & & & \\ & & & \Phi_{\Delta N} & & & & & \\ & & & & . & & & & \\ & & & & & \Phi_{\Delta N} & & & \\ & \mathbf{0} & & & & & \Phi_\gamma & & \\ & & & & & & & . & \\ & & & & & & & & \Phi_\gamma \end{pmatrix} \tag{17}$$

$$\mathbf{P}_0 = \begin{pmatrix} \sigma^2_{dx} & & & & & & & & \\ & \sigma^2_{dy} & & & & & & & \\ & & \sigma^2_{dz} & & & \mathbf{0} & & & \\ & & & \sigma^2_{N^1} & & & & & \\ & & & & . & & & & \\ & & & & & \sigma^2_{N^{K-1}} & & & \\ & \mathbf{0} & & & & & \sigma^2_{\gamma^1} & & \\ & & & & & & & . & \\ & & & & & & & & \sigma^2_{\gamma^{K-1}} \end{pmatrix} \tag{18}$$

$$\mathbf{R} = \begin{pmatrix} \mathbf{D}\mathbf{R}_\rho\mathbf{D}^T & \\ & \mathbf{D}\mathbf{R}_\phi\mathbf{D}^T \end{pmatrix} \tag{19}$$

$$\mathbf{D} = \begin{pmatrix} 1 & -1 & & \\ 1 & & . & \\ . & & & . \\ . & & & & . \\ 1 & & & & -1 \end{pmatrix} \tag{20}$$

$$\mathbf{R}_\rho = diag(2{\sigma^1_\rho}^2, ..., 2{\sigma^{K-1}_\rho}^2) \tag{21}$$

$$\mathbf{R}_\phi = diag(2{\sigma^1_\phi}^2, ..., 2{\sigma^{K-1}_\phi}^2) \tag{22}$$

$$\mathbf{x}_i^- = \mathbf{B}\mathbf{x}_{i-1} \tag{23}$$

$$\mathbf{P}_i^- = \mathbf{B}\mathbf{P}_{i-1}\mathbf{B}^\mathbf{T} + \mathbf{Q} \tag{24}$$

$$\mathbf{z}_i = \mathbf{y}_i - \mathbf{F}\mathbf{x}_i^- \tag{25}$$

$$\mathbf{K}_i = \mathbf{P}_i^-\mathbf{F}\left(\mathbf{F}\mathbf{P}_i^-\mathbf{F}^T + \mathbf{R}\right)^{-\mathbf{1}} \tag{26}$$

$$\mathbf{x}_i^+ = \mathbf{x}_i^- + \mathbf{K}_i\mathbf{z}_i \tag{27}$$

$$\mathbf{P}_i^+ = \left(\mathbf{I} - \mathbf{K}_i\mathbf{F}\right)\mathbf{P}_i^- \tag{28}$$

3. LAMBDA-method based sub-carrier ambiguity resolution

The sub-carrier pseudoranges are ambiguous up to an integer multiple of the sub-carrier wavelength. This ambiguity can be resolved in the position domain by using the LAMBDA ambiguity fixing method. Within this investigation, the LAMBDA method has been implemented by using the LAMBDA software package which was originally developed at TU Delft [10] [11]. In the standard implementation of the LAMBDA method [12], the float ambiguities are taken as an input which are first decorrelated by applying Cholesky Decomposition (Eqn. 29) and by applying Z-transformation to reparameterize the float ambiguities vector $\mathbf{\Delta N}$ (Eqn. 30) and its covariance matrix $\mathbf{Q_{\Delta N}}$ (Eqn. 31). The Z-transform matrix $\mathbf{Z}$ is obtained through an iterative process as described in [13]. After the float ambiguity vector and covariance matrix are decorrelated, a mapping function is used to obtain the integer valued estimate. For an integer-least-squares (ILS), the integer estimate $\widetilde{\mathbf{z}}$ for a float ambiguity vector is obtained by solving the minimization problem in Eqn. 32. This step is realized by performing an integer search to determine $\widetilde{\mathbf{z}}$. The decorrelating Z-transformation largely reduces the search time. The integer estimate is obtained through a search over the integer grid points of an n-dimensional hyper-ellipsoid which has a size defined by a positive constant X^2, is centred at $\bar{\mathbf{z}}$ and is shaped by the covariance matrix $\mathbf{Q_z}$. The integer grid point $\mathbf{z}$ inside the hyper-ellipsoid, which gives the minimum value of function $F(\mathbf{z})$, is the optimal ILS solution for $\widetilde{\mathbf{z}}$. An alternative search strategy based on shrinking the search ellipsoid during the search is proposed in [13] and [11] and also used within the implemented LAMBDA method. After the search process is completed, the fixed ambiguity vector is finally obtained by taking the inverse Z-transform of the searched solution as in Eqn. 34.

$$\mathbf{Q_{\Delta N}} = \mathbf{L}^T\mathbf{D}\mathbf{L} \tag{29}$$

$$\bar{\mathbf{z}} = \mathbf{Z}^T\,\mathbf{\Delta N} \tag{30}$$

$$\mathbf{Q_z} = \mathbf{Z}^T\mathbf{Q_{\Delta N}}\mathbf{Z} \tag{31}$$

$$\widetilde{\mathbf{z}} = \arg\ min\left(\bar{\mathbf{z}} - \mathbf{z}\right)^T\mathbf{Q_z}^{-\mathbf{1}}\left(\bar{\mathbf{z}} - \mathbf{z}\right) \tag{32}$$

$$F(\mathbf{z}) = \left(\bar{\mathbf{z}} - \mathbf{z}\right)^{\mathbf{T}}\mathbf{Q_z}^{-\mathbf{1}}\left(\bar{\mathbf{z}} - \mathbf{z}\right) \leq X^2 \tag{33}$$

$$\widetilde{\Delta\mathbf{N}} = \mathbf{Z}^{-T}\widetilde{\mathbf{z}} \tag{34}$$

As part of this investigation, however, it was noted that the input float ambiguity covariance matrix $\mathbf{Q_{\Delta N}}$ was highly ill-conditioned for the considered datasets. This resulted in candidate integer vector solutions with incorrect absolute values when the back Z-transformation was applied. However, the norms of the fixed integer candidate vectors obtained from this transformation were still useful for applying a ratio and difference based ambiguity resolution test to validate the fixed solution. Hence, within this filter implementation, the back-transformed integer candidate vectors in $\widetilde{\mathbf{\Delta N}}$ are only used to form the ambiguity fixing ratio (Eqn. 35) and difference (Eqn. 36) [14] and not for updating the fixed ambiguity solution. The ratio and difference are compared against their thresholds μ_{ratio} and μ_{diff} respectively. Whenever the thresholds are crossed, a simple rounded solution of the float ambiguity vector is taken as the fixed solution as expressed in Eqn. 37.

$$ratio = \frac{(\widetilde{\mathbf{\Delta N}}_2 - \mathbf{\Delta N})^T\mathbf{Q_{\Delta N}}^{-1}(\widetilde{\mathbf{\Delta N}}_2 - \mathbf{\Delta N})}{(\widetilde{\mathbf{\Delta N}}_1 - \mathbf{\Delta N})^T\mathbf{Q_{\Delta N}}^{-1}(\widetilde{\mathbf{\Delta N}}_1 - \mathbf{\Delta N})} > \mu_{ratio} \tag{35}$$

$$difference = (\widetilde{\mathbf{\Delta N}}_2 - \mathbf{\Delta N})^T\mathbf{Q_{\Delta N}}^{-1}(\widetilde{\mathbf{\Delta N}}_2 - \mathbf{\Delta N}) - (\widetilde{\mathbf{\Delta N}}_1 - \mathbf{\Delta N})^T\mathbf{Q_{\Delta N}}^{-1}(\widetilde{\mathbf{\Delta N}}_1 - \mathbf{\Delta N}) > \mu_{diff} \tag{36}$$

$$\overline{\mathbf{\Delta N}} = round(\mathbf{\Delta N}) \tag{37}$$

4. Fixed solution update

At the output of the LAMBDA block, the fixed ambiguities are obtained. If the fixed ambiguities are correctly resolved, then the position error solution shall be as accurate as the sub-carrier measurement noise. Due to the low measurement noise of the sub-carrier observations, a significant gain in position accuracy can be achieved by conditionally using the fixed ambiguities for position estimate update. The position states and position state covariance matrix are updated according to Eqn. 38 and 39 respectively and where $m : [1, 3]$ and $n : [1, 3]$.

$$\overline{\begin{pmatrix}\delta x\\ \delta y\\ \delta z\end{pmatrix}}_i^+ = \left(\mathbf{H^T Q_y}^{-1}\mathbf{H}\right)\mathbf{H^T Q_y}^{-1}\left(\mathbf{y}_i - \mathbf{A}_\lambda\left(\overline{\mathbf{\Delta N}} - \mathbf{\Delta N}\right)\right) \tag{38}$$

$$\overline{\mathbf{P}_{m,n}{}^+}_i = \mathbf{P}_{m,n}{}^+{}_i - \mathbf{Q_{r\Delta N}}\mathbf{Q}_{\mathbf{\Delta N}}^{-1}\mathbf{Q^T}_{\mathbf{r\Delta N}} \tag{39}$$

5. Absolute solution update

The differential position states are used to update the absolute receiver position $\vec{\mathbf{r}}$ according to Eqn. 40, the differential BSSD sub-carrier ambiguities states are used to update the float ambiguity vector $\mathbf{\Delta N}$ as in Eqn. 41 and the differential BSSD code multipath states are used to update the float ambiguity vector $\mathbf{\Delta}\gamma$ as in Eqn. 42.

$$\vec{\mathbf{r}}_i = \vec{\mathbf{r}}_{i-1} + \begin{pmatrix}\delta x\\ \delta y\\ \delta z\end{pmatrix}_i^+ \tag{40}$$

$$\mathbf{\Delta N}_i = \mathbf{\Delta N}_{i-1} + \begin{pmatrix}\delta\Delta N^1\\ \cdot\\ \cdot\\ \delta\Delta N^{K-1}\end{pmatrix}_i^+ \tag{41}$$

$$\mathbf{\Delta}\gamma_i = \mathbf{\Delta}\gamma_{i-1} + \begin{pmatrix}\delta\Delta\gamma^1\\ \cdot\\ \cdot\\ \delta\Delta\gamma^{K-1}\end{pmatrix}_i^+ \tag{42}$$

III. SIGNAL PLAN AND SIMULATION APPROACH

The assumed signal composition comprises of a high frequency component in addition to a BOC(1,1) signal in order to form a meta-signal with one of the side lobes of the BOC(1,1) component. The high-frequency component is assumed to be modulated with BPSK(1) and to have a chip rate of 1.023 Mcps. The signal power is assumed to be one half of the BOC(1,1) component. The assumed signal structure is hypothetically derived for investigative purposes and is not related to any signal option of a future GNSS signal.

Within the scope of this research work, a simulation framework of Airbus Defence and Space (ADS), called PIPE, and the above described meta-signal positioning engine implemented by the Universität der Bundeswehr München (UniBw) have been used.

Here, PIPE is utilized:

- to generate the required user trajectories
- to generate the corresponding received GNSS signals based on information about the current GNSS constellation (RINEX file), the assumed satellite EIRP, and the receiver antenna pattern. In addition, distortions, such as multipath components, are added.
- to acquire and track the received signals and derive corresponding pseudorange measurements, which are stored in a file together with information about the atmospheric distortions (ionosphere, troposphere) and broadcast group delay for provision to the meta-signal positioning engine

The provided measurements drive the meta-signal processing chain as shown in Fig. 1.

In order to be able to utilize PIPE without implementing any extensions, the signal generation is done by approximating the assumed meta-signal structure as a high order BOC signal. The generation process consists of generating two signals components – a BOC(1,1) component and a BOC(10.75,1) component. Both the components contain the same navigation message. The signal plan in complex baseband domain is illustrated in Fig. 2. Furthermore, it is neglected that the BOC(10.75,1) component is using a complex (cos/sin) sub-carrier. However, only a minor impact of this on the acquisition and tracking performance is expected.

Since an appropriate modified Double-Estimator block for meta-signal tracking is not available in the PIPE simulator, the BOC(1,1) and BOC(10.75,1) signals are independently tracked using a classic early-late correlator tracking scheme supplemented by the Bump Jump algorithm and corresponding pseudoranges are generated for delivery to the meta-signal positioning engine. Overall we have the following emulation of meta-signal tracking:

- **Metasignal code pseudorange from DLL**: emulated via DLL tracking of the BOC(1,1) comoponent
- **Metasignal subcarrier pseudorange from SLL for a OBPSK signal**: emulated via BOC(10.75,1) tracking using a Bump Jumper

The resulting Auto-Correlation Functions (ACF) for both BOC signals, assuming no distortions, are shown in Fig. 3.

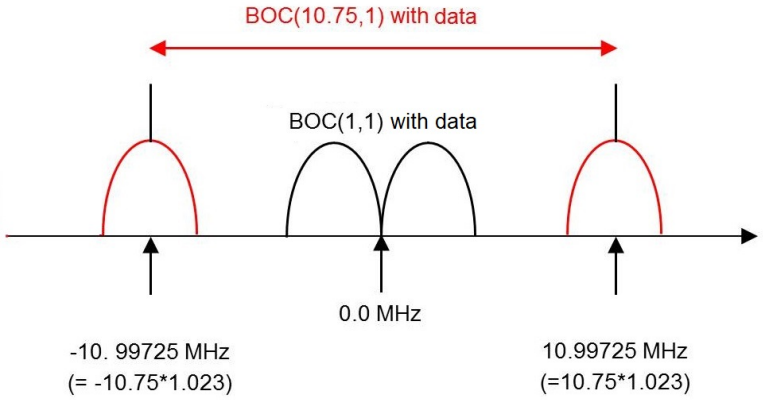

Figure 2: Simulated signal occupancy in complex baseband

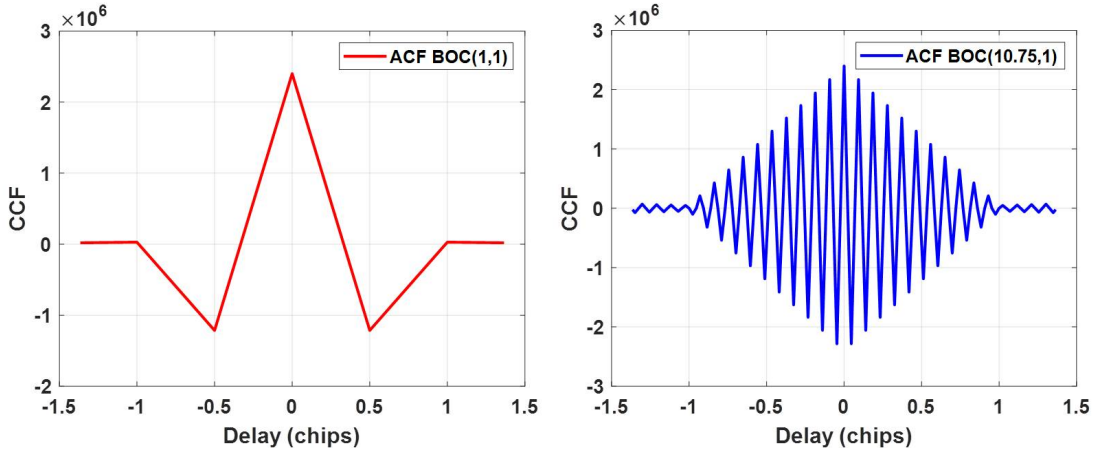

Figure 3: Autocorrelation function (ACF) of BOC(1,1) (left figure) and BOC(10.75,1) (right figure)

IV. TEST CASE PARAMETERS

This section presents the signal generation and Kalman filter parameters for each generated test case. The three considered test cases mainly differ in the assumed channel conditions. The receiver is assumed to be stationary and located close the south-eastern city limit of Munich, Germany. The positions of the visible satellites are based on a MGEX RINEX navigation file dated 02/07/2019.

Both signals of each satellite are tracked independently of each other by applying a second-order DLL with 5 Hz bandwidth and a FLL assisted PLL with 10 Hz (FLL) / 15 Hz (PLL) bandwidth. In addition, a Bump Jump algorithm is applied to suppress side-peak tracking.

Each test case is characterized by a different simulated multipath set-up which is summarized in Table 1. Code and sub-carrier observation from a total of 08 satellites are used for processing the receiver position. Within the filter, the initial receiver position is set to a code-only filtered SPP solution of [4183728.51371908 m, 862903.006111310 m, 4721100.09827803 m] which has a position error of [-16.9959264402278 m, -14.6816836820217 m, 0.226905060000718 m] in the X, Y and Z directions respectively.

Table 1: Summary of test cases with multi-path set-up

Testcase index	Multipath set-up
1	Multipath free test case with 8 satellites characterized by no multipath on code and sub-carrier observations
2	Dynamic multipath on all of the 08 satellites simulated as White Gaussian noise characterized by $\mathcal{N}(0,\, \sigma_C)$ for code and $\mathcal{N}(0,\, \sigma_{SC})$ for sub-carrier observations where $\sigma_C = 10$ m and $\sigma_{SC} = 0.03$ m
3	Strong static multipath on 05 out of 08 satellites with code bias upto 40 m (refer to Appendix for a table with detailed parameters)

For each test case, in a separate experimental run, the filter is reset after 10 secs every time a position fix is achieved to analyse filter stability. Upon filter reset the receiver position is set back to the SPP solution, all the ambiguities states are set to 0.5 (a non-integer value) and the code multipath states are set to 0.

The initial position state-variances $\sigma^2_{dx}, \sigma^2_{dy}$ and σ^2_{dz} are set to 20^2 [m^2] as the filtered SPP solution is accurate to within this limit in each of the X, Y and Z directions. The position state-process noise $\Phi_{\delta x}, \Phi_{\delta y}$ and $\Phi_{\delta z}$ are tuned to a low value of 0.00015^2 [m^2] considering a static-receiver case.

The initial ambiguity state-variance $\sigma^2_{N^k}$ is set to $(10\lambda)^2$ [m^2] as a maximum sub-carrier ambiguity of 10 is assumed, implying a worst-case sub-carrier lock on the 10th side-peak.

The initial code multipath state-variance $\sigma^2_{\gamma^k}$ and code multipath state-process noise Φ_γ are tuned to obtain the best results for different code bias present in each test case. These are different for the test cases.

A two threshold based ambiguity fixing scheme is considered in which the ambiguities are considered fixed if the ratio and difference of the first two candidate vector norms exceed their corresponding threshold μ_{ratio} and μ_{diff} respectively. The values of the threshold were observed to highly influence the fixing time and number of correct/incorrect fixing and hence are different for the test cases.

V. POSITIONING RESULTS

1. **Testcase 1** (refer to Fig. 4 and Fig. 5)

   With no filter reset, all ambiguities instantaneously fix to 0. With reset, all ambiguities are correctly fixed in the 2nd epoch after reset. It takes at least one epoch to compute the differential float ambiguities that need to be added as offsets to the absolute float ambiguities before fixing can take place.

2. **Testcase 2** (refer to Fig. 6 and Fig. 7)

   With no reset, all ambiguities fix to 0 at about t = 30 s. The filter convergence time is higher in comparison to Testcase 1 because of the presence of multipath. However, upon successful fixing, the horizontal and vertical position error shows no bias. This is because the multipath in this case is simulated as White Gaussian noise with zero mean. When the fixed solution is used, the position error is as accurate as the sub-carrier measurement noise which is in the dm level.

Table 2: Kalman filter parameters for Testcase 1, 2 and 3

Parameter	Symbol	Value		
		Testcase 1	**Testcase 2**	**Testcase 3**
Initial position state variance	$\sigma^2_{dx}, \sigma^2_{dy}, \sigma^2_{dz}$	20^2 [m^2]	20^2 [m^2]	20^2 [m^2]
Initial ambiguity state variance	$\sigma^2_{N^k}$	$(10\lambda)^2$ [m^2]	$(10\lambda)^2$ [m^2]	$(10\lambda)^2$ [m^2]
Initial code multipath state variance	$\sigma^2_{\gamma^k}$	5^2 [m^2]	5^2 [m^2]	10^2 [m^2]
Position process noise	$\Phi_{\delta x}, \Phi_{\delta y}, \Phi_{\delta z}$	0.00015^2 [m^2]	0.00015^2 [m^2]	0.00015^2 [m^2]
Code multipath process noise	Φ_γ	1^2 [m^2]	1^2 [m^2]	5^2 [m^2]
Code measurement noise variance	σ^2_ρ	5^2 [m^2]	5^2 [m^2]	5^2 [m^2]
Sub-carrier measurement variance	σ^2_ϕ	0.088^2 [m^2]	0.088^2 [m^2]	0.088^2 [m^2]
Ambiguity resolution ratio threshold	μ_{ratio}	1	1	1
Ambiguity resolution difference threshold	μ_{diff}	0	$2.5e3$	$1e3$

3. **Testcase 3** (refer to Fig. 8 and Fig. 9)

   With no reset, as the ambiguities are fixed, all the error in the float solution is accumulated and distributed over the code MP states which produces a jump in the code residuals (at t = 80 s in Fig. 8) which then converges to the true static code MP values over time. However, since after fixing, the position error is as accurate as the sub-carrier measurement noise, this large residual in code MP states does not negatively impact the result.

   The filter convergence time is higher than Testcase 1 and 2 due to the presence of strong static multipath with code bias up to 40 m for some satellites.

   Upon successful fixing, the horizontal position error is biased up to 1m in the North direction and 3m in the East direction. The vertical position error is biased up to 1m. This bias in the position error can be attributed to the lower quality of code observations and to the unaccounted multipath in the sub-carrier observations. Within this filter implementation, the multipath in the sub-carrier observation is not estimated. Upon successful ambiguity fixing the sub-carrier multipath delay is absorbed in the estimated receiver position and sub-carrier residuals.

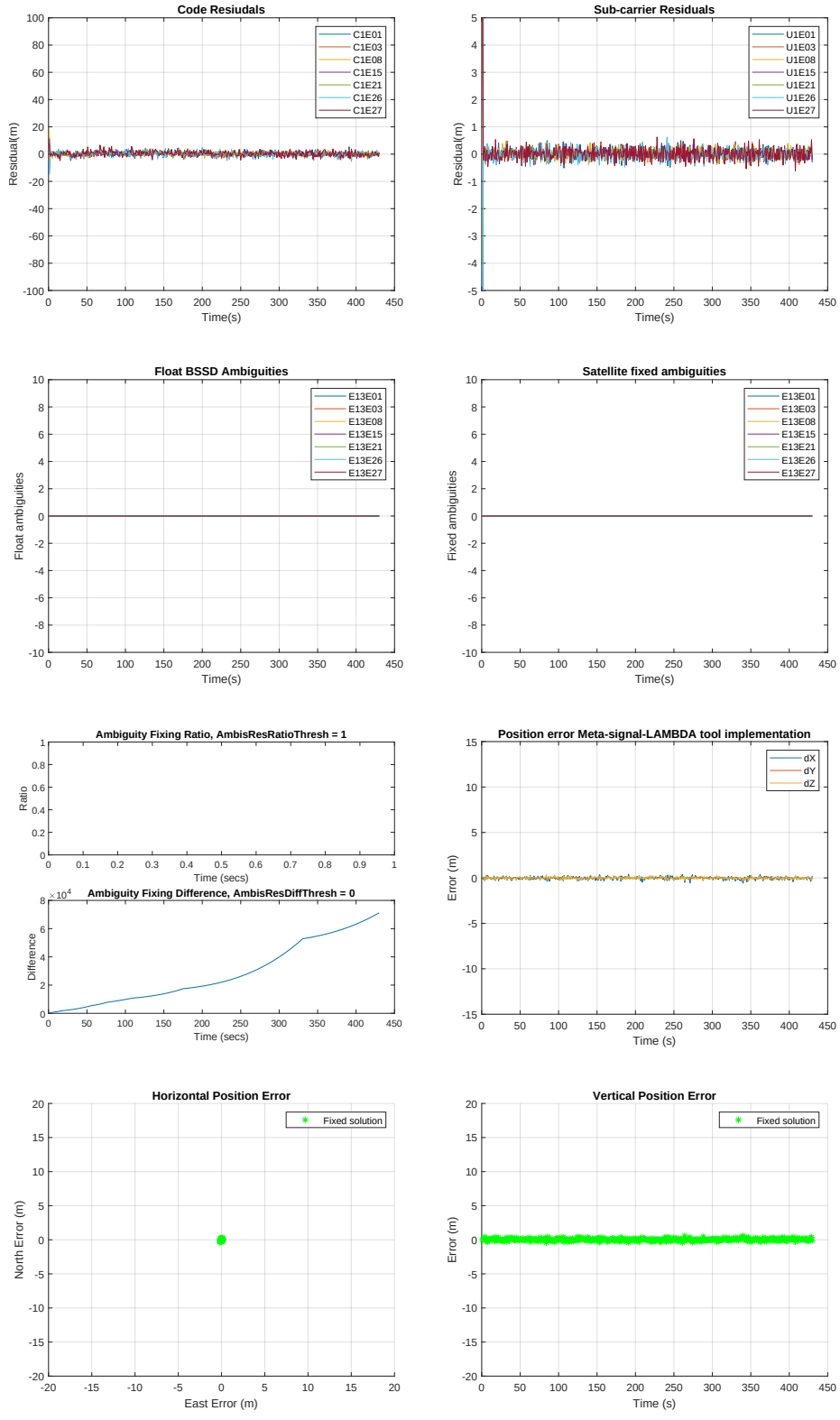

Figure 4: Positioning results for Test case 1

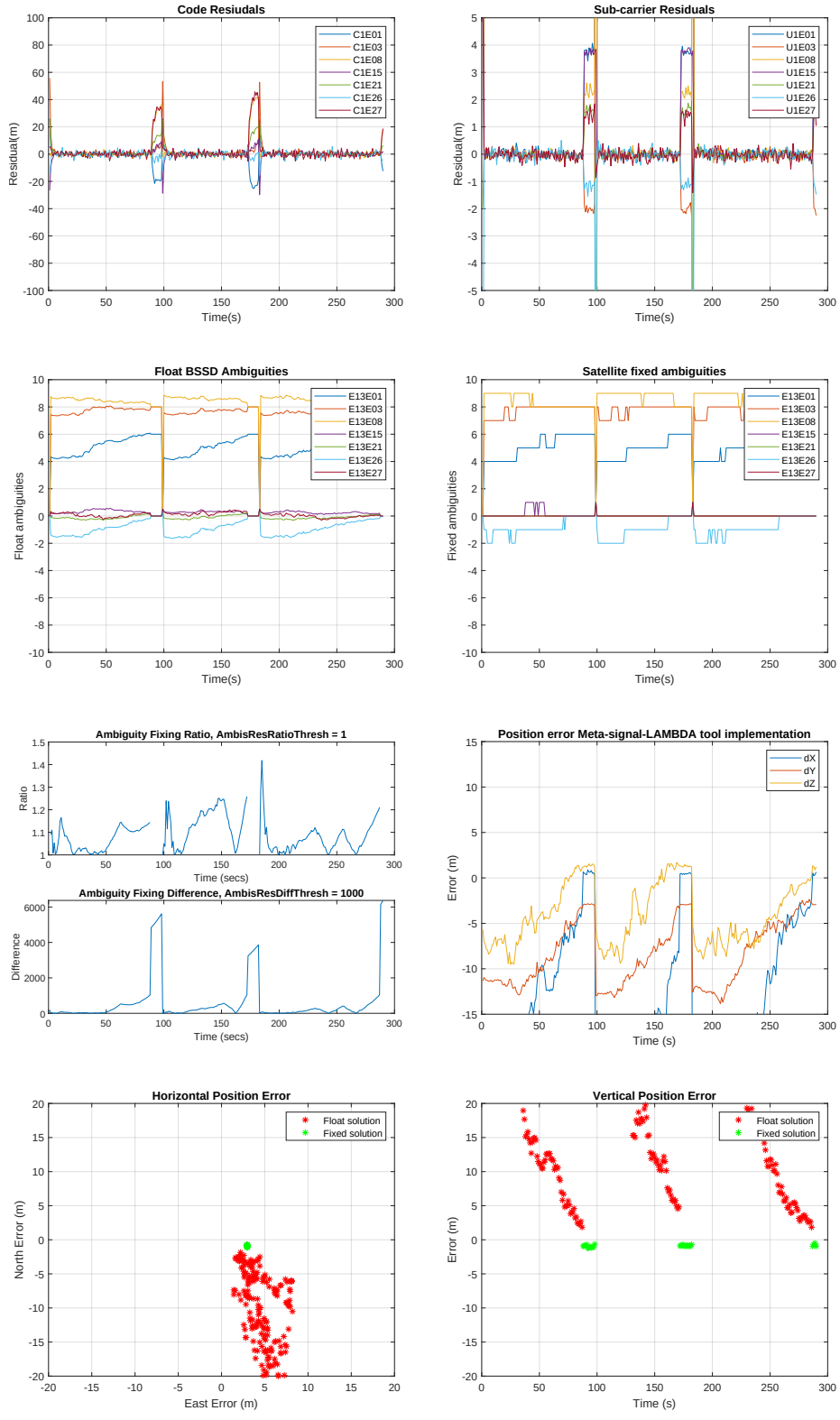

Figure 5: Positioning results for Test case 1 with filter reset

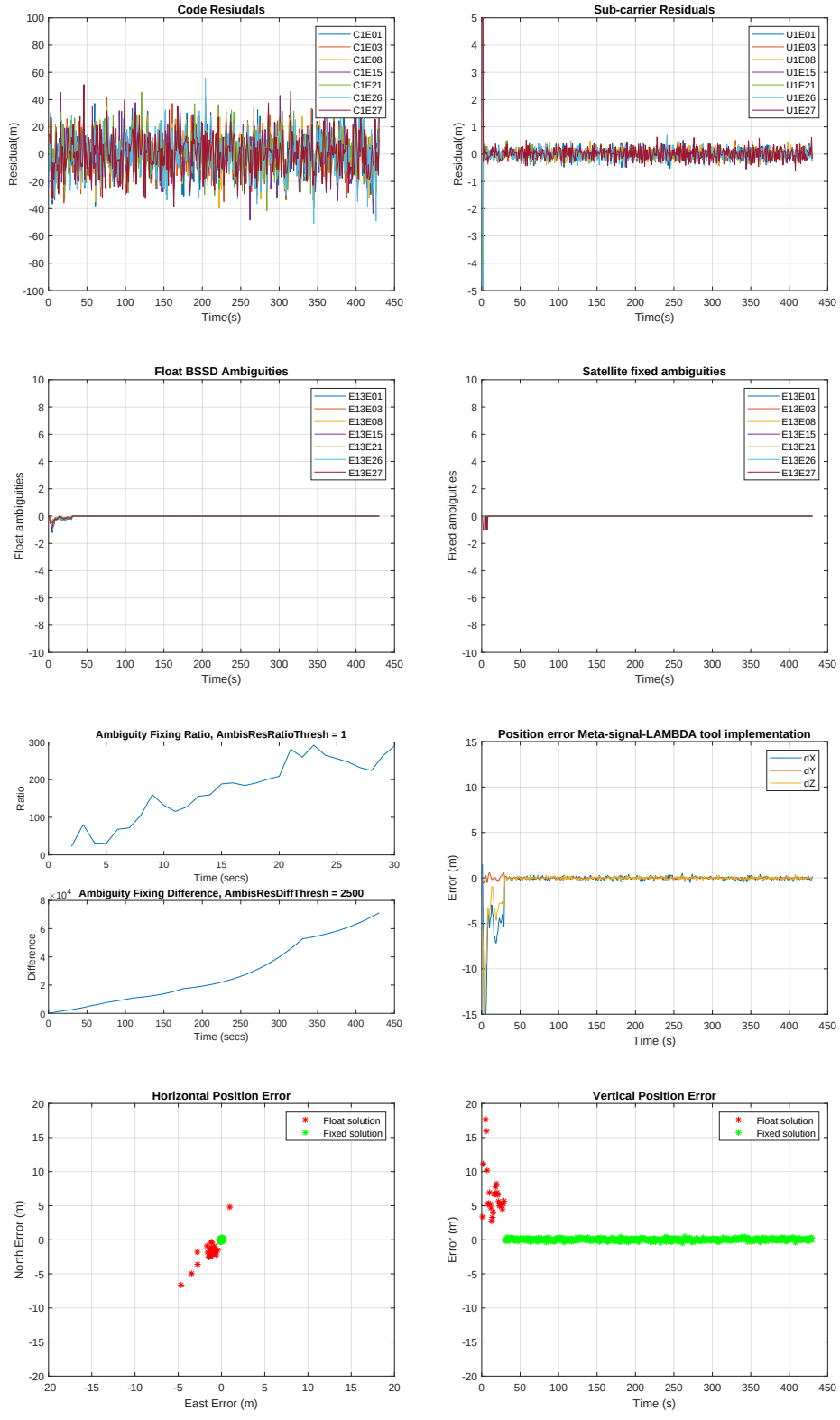

Figure 6: Positioning results for Test case 2

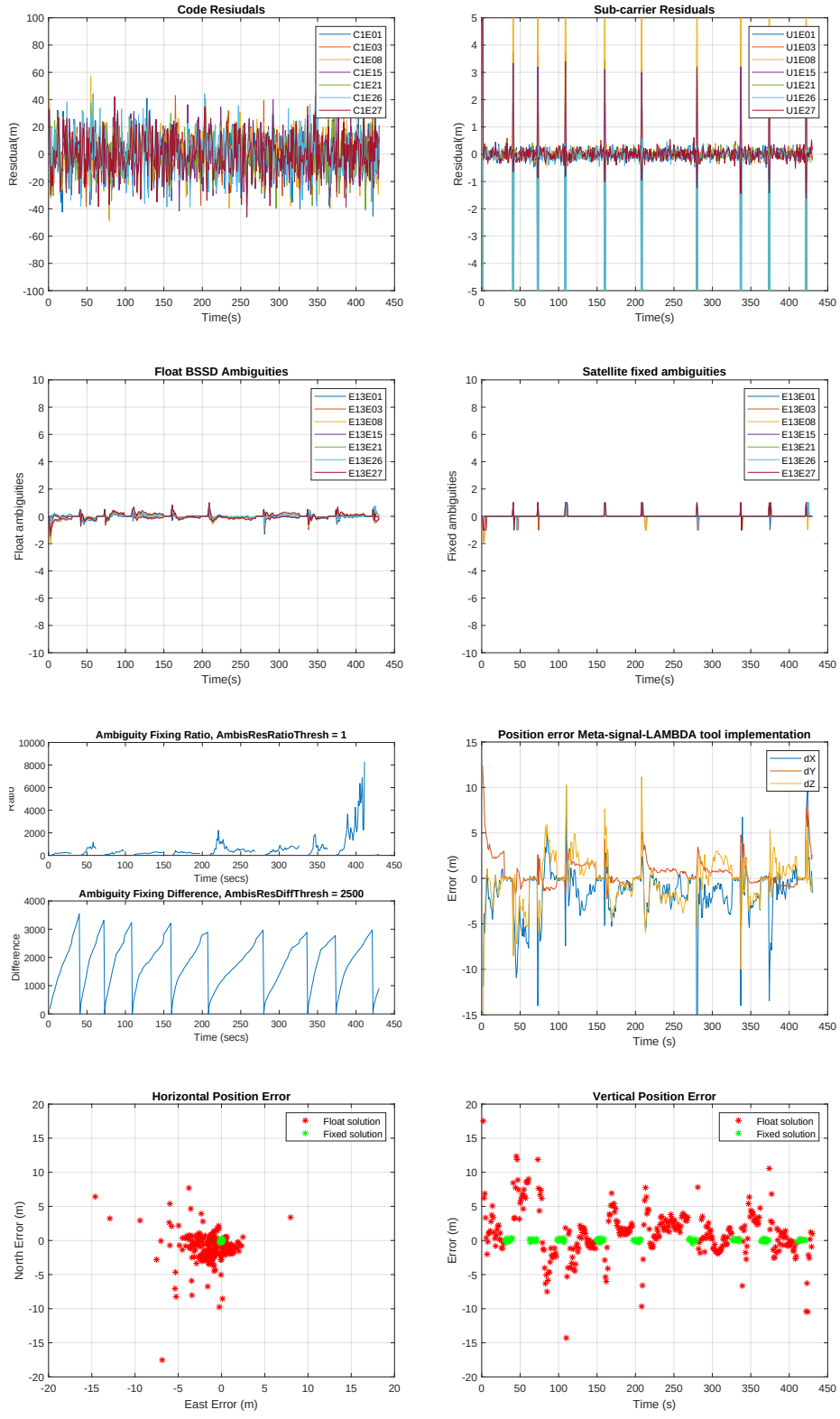

Figure 7: Positioning results for Test case 2 with filter reset

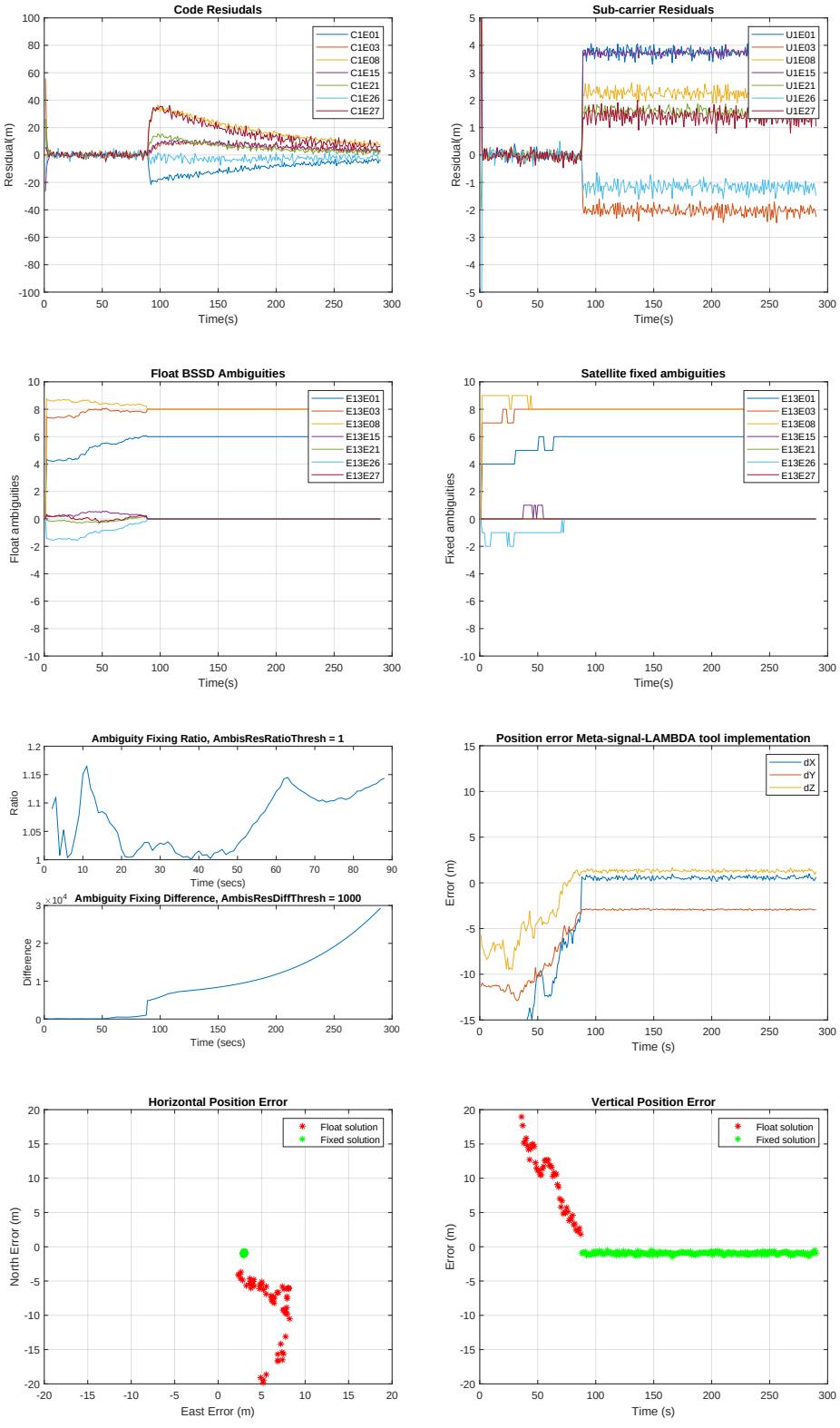

Figure 8: Positioning results for Test case 3

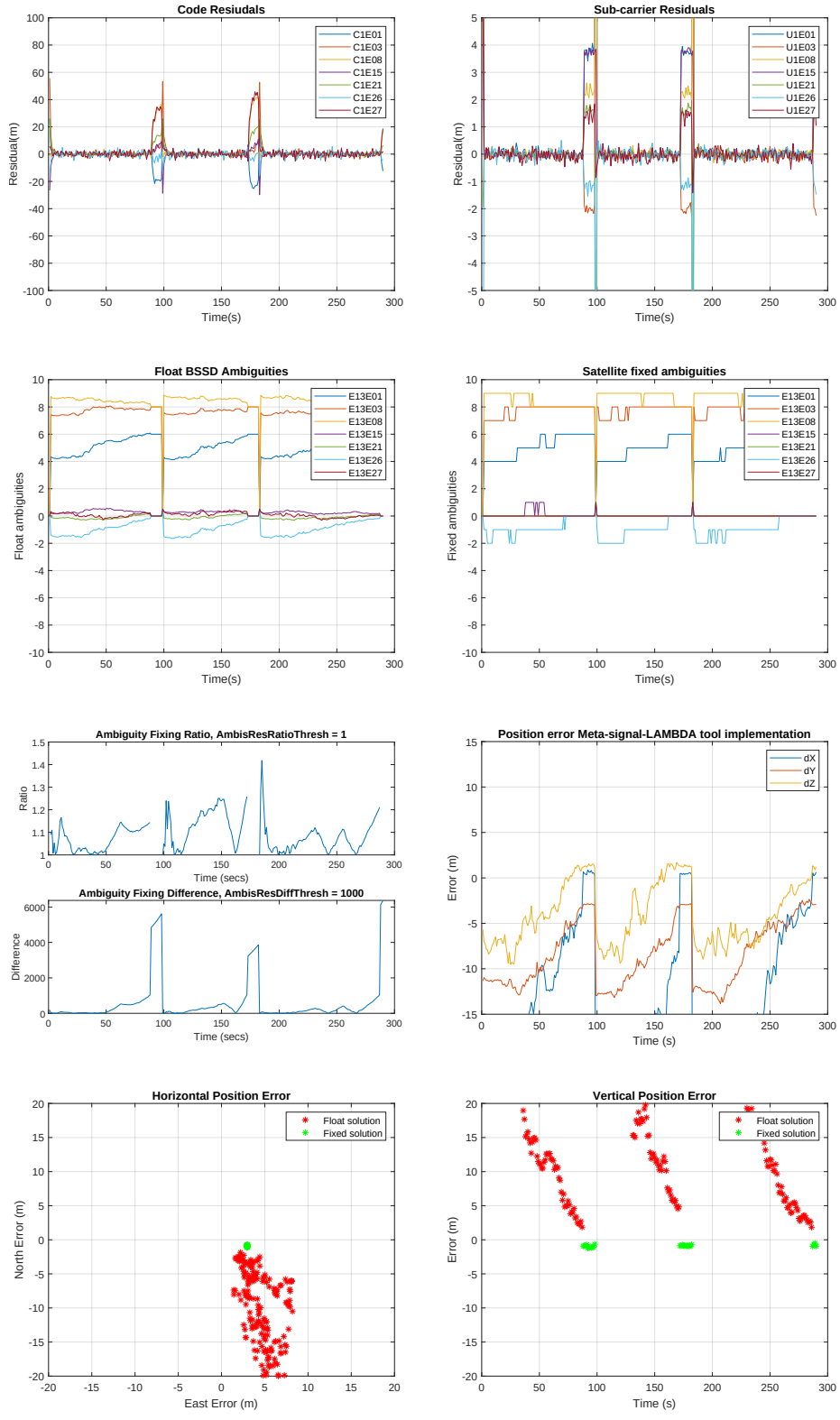

Figure 9: Positioning results for Test case 3 with filter reset

VI. CONCLUSIONS

Overall, as part of this research work, the feasibility of using LAMBDA ambiguity fixing method for sub-carrier ambiguity fixing has been demonstrated by implementing a Kalman filter based meta-signal positioning engine. As a primary outcome of the demonstration, it can be concluded that LAMBDA ambiguity fixing can successfully resolve sub-carrier ambiguities, even in high static multipath scenarios, given that a suitable filter is employed.

For the considered test cases with simulated multipath, it was deemed essential that the code multipath should be estimated in order to obtain correct results for sub-carrier ambiguity fixing. With no estimation of code multipath delay, the BSSD sub-carrier ambiguities were observed to be fixed to incorrect values. Hence, the code multipath differential offsets were included in the Kalman filter state-vector within this investigation.

Moreover, the filter convergence time for correct ambiguity fixing is observed to be highly dependent on the quality of code observations with higher code multipath resulting in higher convergence time. This implies that in urban canyon environments, it would be reasonable to allow some initial time duration to condition sub-carrier observations on filtered code observations before the actual fixing takes place.

With correct fixing, sub-carrier ambiguity resolution in position domain can realize dm level accurate position solutions without RTK methods i.e without the requirement a reference receiver. For a full-scale standardization of sub-carrier observations, the RINEX file format has to be updated with a dedicated sub-carrier observation tag.

Lastly, it has to be emphasized that sub-carrier fixing at range level produced similar results with Bump Jump or rounding of Double Estimator SLL output for low multipath scenarios. However, in the case of a high-multipath scenario, such as the one simulated in Testcase 3,the LAMBDA method displayed improved results. Having said this, there is a need of further consolidation with processing of multiple datasets that realize a dynamic user scenario and more realistic channel conditions.

APPENDIX

Strong multipath scenario parameters

Table 3 summarizes the "strong" multipath parameters for the five satellites. Both signals of each satellite (BOC(1,1) as well as BOC(10.75,1)) are assumed to be distorted by the same specular reflection, which is static and as a consequence, can be characterized by the relative amplitude, the relative delay and relative phase with respect to the direct path.

Table 3: Summary of parameters for the strong multipath scenario

PRN Number	Relative Amplitude	Relative Delay [m]	Relative Phase [rad]
01	0.9	90.0	0.0
03	0.9	100.0	0.0
08	0.9	120.0	π
15	0.9	70.0	π
21	0.9	60.0	0.0

The impact of the static multipath component on the auto-correlation function is exemplary shown in Fig. 10 for the multipath parameters applied to the PRN08 signals. The difference compared to the curves in Fig. 3 without multipath component can be easily recognized. The distorted ACF of the BOC(1,1) signal leads to a bias in the corresponding code phase tracking of about 18 m. However, no side-peak tracking was recognized. In contrast, side-peak tracking was observed for the BOC(10.75,1) signal, which can be explained with the help of Fig. 11 showing a magnified version of the ACF around zero delay. There is a side-peak located at a delay of 0.36 (BOC(1,1)) chips that is larger than the two neighboring peaks. Due to this situation, the sub-carrier phase tracking can be stuck at this side-peak, even when the Bump Jump algorithm is applied and, as a consequence, a sub-carrier phase tracking bias of about 105 m is observed.

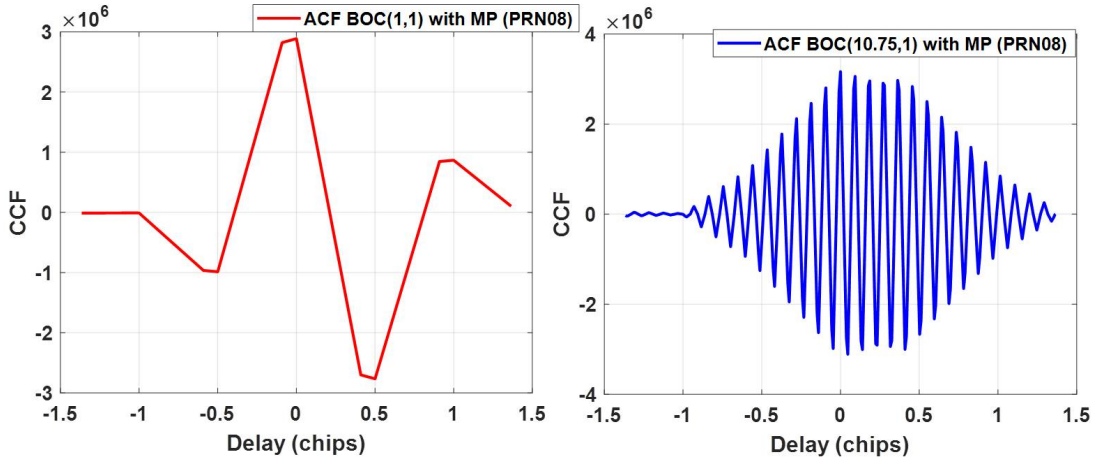

Figure 10: Exemplary autocorrelation function (ACF) of BOC(1,1) (left figure) and BOC(10.75,1) (right figure) assuming the multipath parameters for PRN08

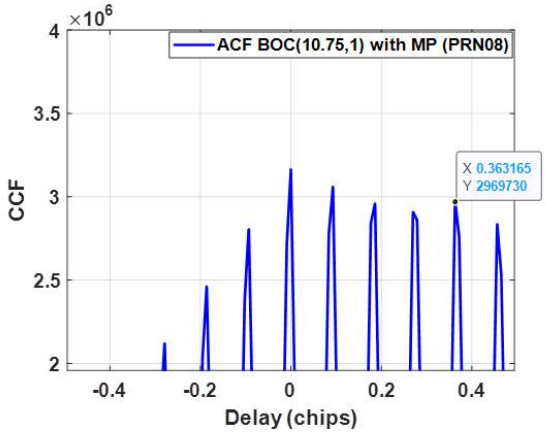

Figure 11: Detail: exemplary autocorrelation function (ACF) of BOC(10.75,1) assuming the multipath parameters for PRN08

REFERENCES

[1] M. Paonni, J. Curran, M. Bavaro, and J. Fortuny-Guasch, "Gnss meta signals: Coherently composite processing of multiple gnss signals," in *Proceedings of the 27th International Technical Meeting of the Satellite Division of The Institute of Navigation (ION GNSS+ 2014)*, 2014, pp. 2592–2601.

[2] J.-L. Issler, M. Paonni, and B. Eissfeller, "Toward centimetric positioning thanks to l-and s-band gnss and to meta-gnss signals," in *2010 5th ESA Workshop on Satellite Navigation Technologies and European Workshop on GNSS Signals and Signal Processing (NAVITEC)*. IEEE, 2010, pp. 1–8.

[3] J. W. Betz, "The offset carrier modulation for gps modernization," in *Proceedings of the 1999 National Technical Meeting of The Institute of Navigation*, 1999, pp. 639–648.

[4] P. Fine and W. Wilson, "Tracking algorithm for gps offset carrier signals," in *Proceedings of the 1999 national technical meeting of The Institute of Navigation*, 1999, pp. 671–676.

[5] C. ODriscoll, J. Avila-Rodriguez, and R. Ioannides, "Subcarrier aided code tracking of high order boc signals," in *Proc. 29th Int. Tech. Meeting Satellite Division Institute Navigation*, 2016.

[6] M. Hodgart, P. Blunt, and M. Unwin, "The optimal dual estimate solution for robust tracking of binary offset carrier (boc) modulation," in *Proceedings of the 20th International Technical Meeting of the Satellite Division of The Institute of Navigation (ION GNSS 2007)*, 2007, pp. 1017–1027.

[7] J. Wendel, F. M. Schubert, and S. Hager, "A robust technique for unambiguous boc tracking," *NAVIGATION*, vol. 61, no. 3, pp. 179–190, 2014. [Online]. Available: https://onlinelibrary.wiley.com/doi/abs/10.1002/navi.62

[8] E. G. N. S. S. Agency, "Gsa gnss market report," 2019.

[9] W. Gurtner and L. Estey, "Rinex-the receiver independent exchange format-version 3.00," *Astronomical Institute, University of Bern and UNAVCO, Bolulder, Colorado.*, 2007.

[10] M. Geodesy and D. U. o. T. Positioning, "Lambda software package : Matlab implementation, version 3.0." [Online]. Available: https://www.tudelft.nl/citg/over-faculteit/afdelingen/geoscience-remote-sensing/research/lambda/lambda

[11] P. De Jonge, C. Tiberius *et al.*, "The lambda method for integer ambiguity estimation: implementation aspects," *Publications of the Delft Computing Centre, LGR-Series*, vol. 12, no. 12, pp. 1–47, 1996.

[12] P. Teunissen, "The least-squares ambiguity decorrelation adjustment: a method for fast gps integer ambiguity estimation," *Journal of geodesy*, vol. 70, pp. 1–2, 1995.

[13] P. J. Teunissen, "Least-squares estimation of the integer gps ambiguities," in *Invited lecture, section IV theory and methodology, IAG general meeting, Beijing, China*, 1993.

[14] L. Wang and S. Verhagen, "A new ambiguity acceptance test threshold determination method with controllable failure rate," *Journal of geodesy*, vol. 89, no. 4, pp. 361–375, 2015.